Density and temperature maps of an aluminium plasma produced by laser ablation

E. Pérez-Tijerina
Facultad de Ciencias Físico-Matemáticas de la Universidad Autónoma de Nuevo León, Apartado Postal 101-F, San Nicolás de los Garza, N.L., 66450, México.

J. Bohigas
Instituto de Astronomía, Univaersidad Nacional Autónoma de México, Apartado Postal 877, Ensenada, B.C. México 22800

R. Machorro
Centro de Ciencias de la Materia Condensada, Univaersidad Nacional Autónoma de México, Apartado Postal 2681 Ensenada, B.C., México 22860

Recibido el 11 de junio de 2004; aceptado el 10 de noviembre de 2004

A wide field spectrograph was used to calculate maps of the electron density and temperature of an aluminium plasma produced by laser ablation. Data were acquired from a single laser pulse. Line widths of singly and doubly ionized aluminium were used to calculate the density from the Stark effect. Temperature was determined using relative line intensities from successive ionization stages. This single pulse, two-dimensional diagnostic of the plasma may contribute to a better understanding of thin film synthesis by pulsed laser deposition.

Keywords: Plasma; spectroscopy; wide field spectroscopy; laser ablation.

En este trabajo se utiliza un espectrógrafo de campo amplio para calcular mapas bidimensionales de la densidad y temperatura del plasma de Aluminio producido por ablación láser. Para calcular la densidad se utilizó el ensanchamiento debido al efecto Stark de líneas de aluminio una y dos veces ionizado. La temperatura se determinó usando intensidades relativas de líneas de estados sucesivos de ionización. Los datos necesarios para generar ambos mapas se adquirieron con un solo pulso del láser. Este tipo de diagnóstico bidimensional usando un solo pulso del láser puede contribuir a un mejor entendimiento del proceso de síntesis de capas delgadas mediante la técnica de ablación láser.

Descriptores: Plasma; espectroscopía; espectroscopía de campo ancho; ablación laser.

PACS: 52.50.Jm; 29.30.-h

1. Introduction

Pulsed laser generated plasmas have a brief existence and their properties are far from uniform. Optical spectroscopy provides information about the spatial and temporal evolution of transient species produced by the laser-target interaction, such as excited atoms, ions or molecules [1]. Information about the laser-target and laser-plasma interactions can be obtained by inspecting volume elements near the target in the early stages of the plasma. The plasma species reactivity, which is essential for thin film formation, is studied at greater distances from the target. Better insights into the dynamics of the ablated material can help understand and eventually control the ablation process [2, 3].

Electron density (n_e) can be determined from the Stark broadening of spectral lines [4–6]. Temperature (T_e) can be found from line intensity ratios from the same or subsequent ionization stages, the ratio of line intensity to the underlying continuum, and by the shape of the continuum spectrum [6]. These are based on the assumption of thermal equilibrium. These quantities can also be found from selected line ratios of the same ionic species under the more general assumption of statistical equilibrium [7].

Optical spectra in the target-substrate direction (axial in this work) have been extensively studied, either point by point [9, 10] or by a linear scanning technique [1, 8]. Good spectral information is obtained, but the spatial resolution is poor. Although scanning in any other direction is feasible, as far as we know this has not been reported. Direct imaging [3], either with or without wide or narrow band filters, is a complementary approach. In this case, the spatial resolution is excellent, and qualitative and morphological information about the plasma is obtained, but the spectral data are minimal.

Here, we present a two-dimensional analysis of the plasma parameters n_e and T_e with a single laser pulse using an optical fiber array attached to a wide-field spectrograph. With this experimental setup, we obtain spatial and spectral information about the plasma simultaneously. Spectral resolution is constrained by the slit width of the spectrograph, which is determined by the optical fiber area (250 μm). The number of inspected regions in the plasma is constrained by the number of fibers (25) that can be placed along the slit length without having spectral overlap at the CCD. Spatial coverage and resolution are limited by the number of the fibers and their area respectively.

2. Experiment

Detailed information concerning the experimental set-up has previously been reported [11]. The plasma is generated by ablation of a high purity Al target, using a 248 nm wavelength

Krypton-Fluor excimer laser with a pulse width of 30 ns. The laser is focused on the target; the spot size is 0.5×1 mm. The target is located at the center of a vacuum chamber. The substrate is 60 mm away from the target.

A quartz lens forms the plume image in the image plane, where an optical fiber array with $N * M = S$ fibers is placed. The array is re-arranged to form a one-dimensional column with S fibers, which become the entrance slit of the spectrograph. A gated image intensified CCD [14] captures the output plane of the spectrograph. An electronic device produces a precise time delay (with set time intervals of 25 ns) between laser pulse and image capture. We used an f/8 commercial spectrograph with a 50 cm focal length and a 2 cm entrance slit, coupled to a 1200 l/mm grating blazed at 500 nm. Its dispersion and resolution are 0.033 nm/pixel and 0.19 nm, respectively. We used 25 optical fibers, each with a 250μm diameter and a 200 μm core. The number of fibers was chosen to avoid spectral overlapping on the CCD.

3. Results and discussion

Stark broadening is mainly dominated by electron impact. Ion perturbations are minor, and the ion correction factor can be neglected. The FWHM $\Delta\lambda_{1/2}$ of the line profile is related to the electron density by the simplified expression [6]

$$\Delta\lambda_{1/2} = 2 \times 10^{-16}\ \mathrm{W}\ n_e. \tag{1}$$

where W is the weakly temperature-dependent electron impact parameter.

We shall calculate n_e using Stark broadening of the Al II 466.3 nm and Al III 452.9 nm emission lines. Spectroscopic constants for these lines are found in [12, 13]

Intensity ratios from lines of the same ion do not provide sufficiently accurate temperatures, due to the relatively small energy difference between the two upper levels. Considerable improvement in sensitivity can be obtained by selecting lines from successive ionization stages, since the effective energy difference is enhanced by the ionization energy. In local thermodynamic equilibrium, the ratio of these line intensities is given in [6]

$$\frac{I'}{I} = \frac{f'g'\lambda^3}{fg\lambda'^3}\left(4\pi^{2/3}a_0^3 n_e\right)^{-1}\left(\frac{kT}{E_H}\right)^{2/3} \times \exp\left(\frac{E' + E_\infty - E - \Delta E_\infty}{kT}\right), \tag{2}$$

The primed symbols are for the higher ionization stage, f is the oscillator strength, g the statistical weight, a_0 the Bohr radius, E_H the ionization energy of the hydrogen atom, E the excitation energy and ΔE_∞ the correction to the ionization energy E_∞ of the lower ionization stage due to plasma interactions. We applied this equation to the Al III 452.9/Al II 466.3 nm ratio to find the plasma temperature. Spectroscopic constants for these lines are from [15].

3.1. Analysis of the plasma in the axial direction

The aluminium plasma was produced with a 400 mJ laser pulse. The spectra were captured 200 ns after the laser trigger, and gate width was set at 50 ns. The fiber array in the image plane consists of 25 fibers aligned in the axial (target-substrate) direction. The output on the ICCD is shown in Fig. 1. Wavelength is drawn along the y-axis, and the spectra produced by all fibers in the array run along the horizontal axis. Notice that Al II 466.3 nm can be seen at longer distances than any other line, indicating that Al II has expanded over a larger volume than Al III (notice that the there is a $\sim 1\mathring{A}$ offset in the wavelength scale). For longer delay times, we find that the Al II lines eventually disappear, suggesting that electron recombination is an important process in the plasma plume.

From the linewidth of the Al II 466.3 nm and Al III 452.9 nm, assumed to be mostly due to Stark broadening, the electron density is estimated at each plasma region sampled by a fiber. The density is plotted in Fig. 2 as a function of target-substrate distance. As expected, it decreases as a function of distance from the target, roughly from 5.5×10^{17} to $10^{17}\mathrm{cm}^{-3}$.

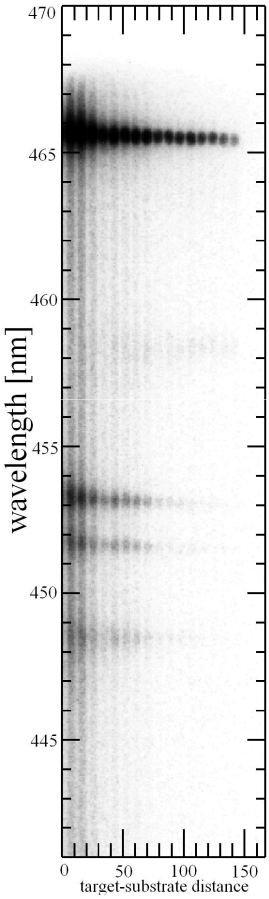

FIGURE 1. Display of the ICCD output with the 25 fibers placed in the target-substrate direction. The spectra were taken with a single pulse.

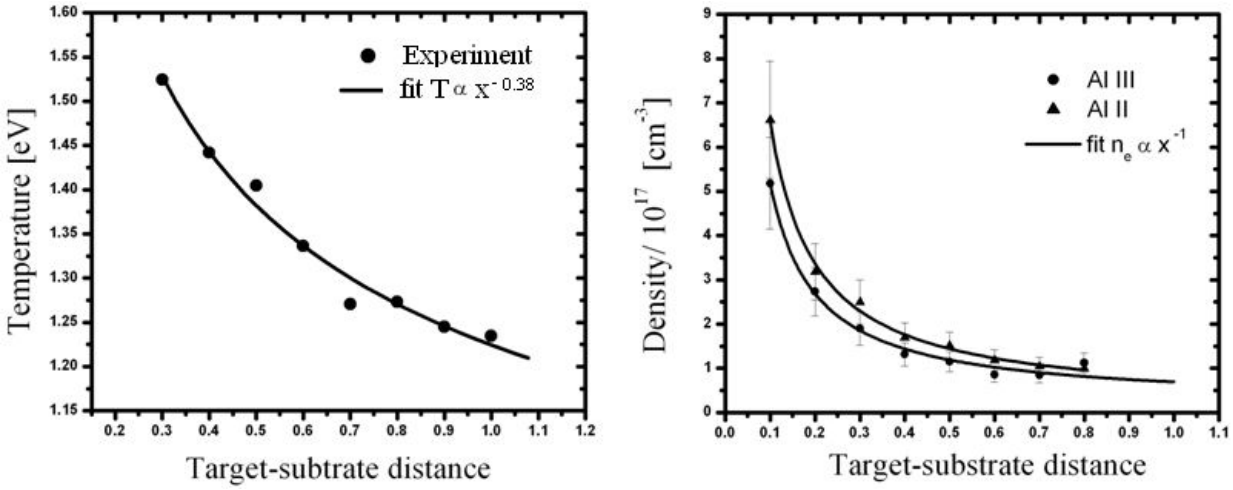

FIGURE 2. Electron density (lower panel) and temperature (upper panel) of the aluminium plasma as a function of distance from the target surface obtained from the spectra shown in Fig. 1. The density was obtained from Al II 466.3 nm and Al III 452.9 nm and the solid line is a x^{-1} fit to the data. Temperature was determined from Al III 452.9/Al II 466.3 nm and the solid line is a $x^{-0.3}$ fit to the data.

The data can be fitted with a function $n_e \propto x^{-1}$, where x is the distance from the target. Notice that, within errors, the same densities are derived from the Al II and Al III lines. This supports our measurements, our assumptions that the plasma is in thermal equilibrium and line broadening is due to the Stark effect, and the accuracy of the Stark analysis.

From the ratio Al III 452.9/Al II 466.3 nm and Eq. 3, we obtain T_e for this plasma along the axial direction. The temperature also falls as we move away from the target (see Fig. 2), changing from 1.55 eV to 1.2 eV in the inspected regions of the plasma plume. The temperature variation as a function of the distance x to the target can be fitted with a $T_e \propto x^{-0.3}$ function. There is full agreement with [1, 9].

3.2. Two-dimensional analysis of the plasma

In this experiment, identical conditions were used to produce the plasma, and the spectra were also acquired 200 ns after the laser pulse. The 25 fibers were placed in a 5×5 array in the image plane, and then re-arranged in a 25 fiber column in the entrance slit of the spectrograph. The two-dimensional end of the array was oriented so that each row is parallel to the axial direction of the plume. Fig. 3 shows the ICCD output of this setup. The first five spectra correspond to the first row in the two-dimensional side of the array, and so on. From these spectra we can now determine the bidimensional variation of n_e and T_e in the plasma, repeating the calculations previously applied to the Al II 466.3 nm and Al III 452.9 nm lines.

In Fig. 4, we present two-dimensional maps for n_e and T_e respectively. The density was determined with the Al II 466.3 line, and the temperature from Al II 466.3/Al III 452.9 nm. These maps were obtained by decoding the fiber arrangement and plotting these quantities at the corresponding position of the plasma image. Since we do not have full spatial resolution, a linear interpolation algorithm was applied to the raw image. Even so, these low spatial resolution images give an

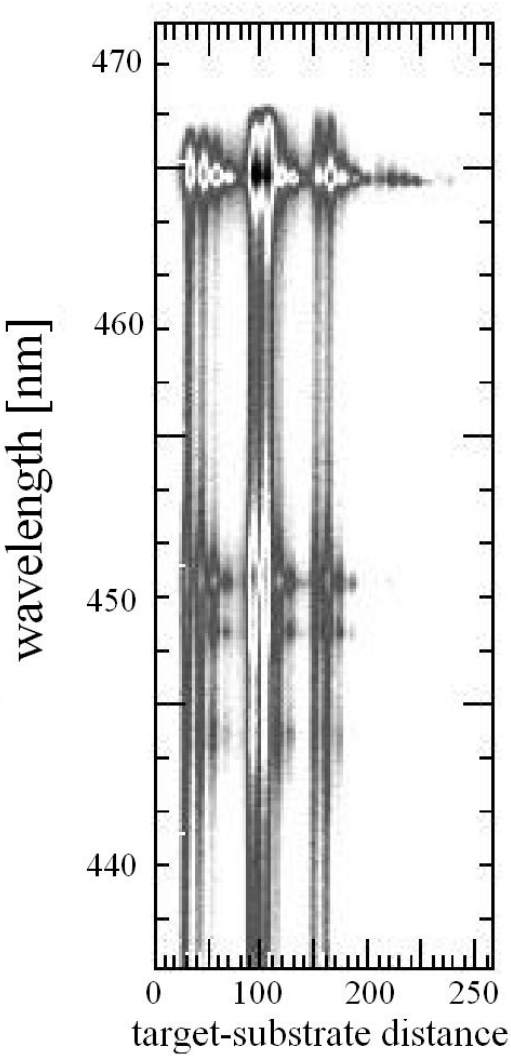

FIGURE 3. Resulting spectra of the experiment conducted with a two-dimensional array placed in the image plane. Each 5 spectra (fibers) it covers the distance target-substrate.

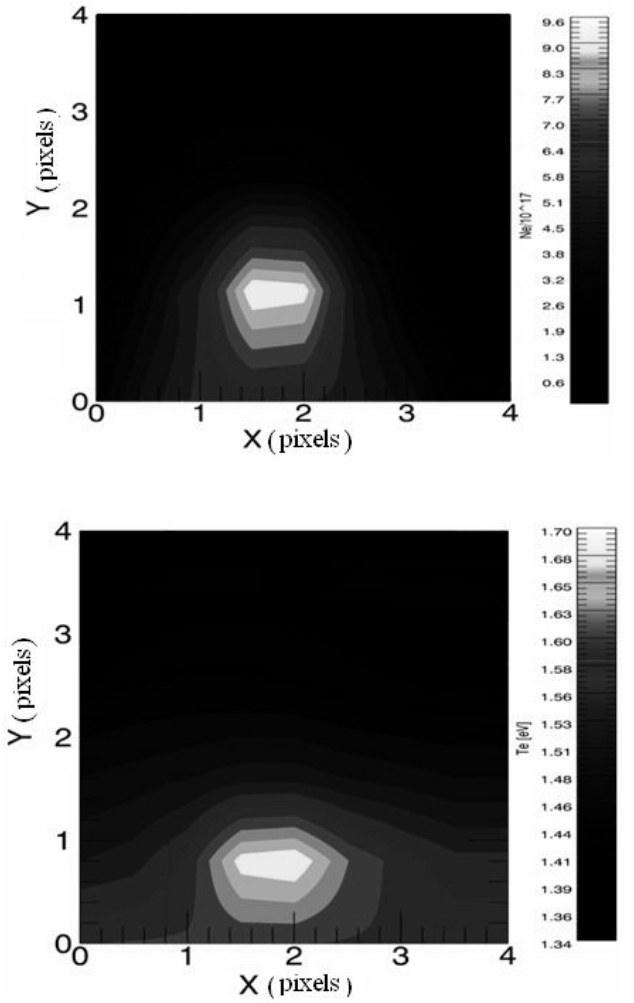

FIGURE 4. Two-dimensional electron density (upper panel) and temperature (lowre panel) maps of the aluminium plasma obtained from the spectra shown in Fig.3. The density was determined from Al II 466.3 nm and temperature from Al III 452.9/Al II 466.3 nm. In this figure each fiber is represented by one pixel.

unprecedented estimate of the two-dimensional behavior of these quantities. The propagation of the entire plasma plume can be followed by capturing its spectra with this array at different delay times.

In the axial direction, the $n_e \propto x^{-1}$ and $T_e \propto x^{-0.3}$ relations were also found. The range of sampled densities, from $9 \times 10^{17}\text{cm}^{-3}$ to $6 \times 10^{16}\text{cm}^{-3}$, is different since we probably measured different plasma regions. Likewise with the temperature, where the measured range is from 1.7 to 1.5 eV. We were not able to derive similar functions in other directions, due to insufficient sampling.

4. Conclusions

A wide field spectrograph was used to analyze the behavior of the electron density and temperature of a laser-produced aluminium plasma. The density was determined from the Stark broadening of aluminium lines from its first and second ionization stages, and results from both lines were identical within experimental error. Temperature was calculated from line intensity ratios of successive ionization stages of aluminium. Profiles of the electron density and temperature in the target-substrate direction were obtained with a fiber array aligned in this direction, and results are consistent with previous reports. A two-dimensional array was constructed to determine for the first time the bidimensional behavior of these quantities from a single laser pulse. It is shown that wide field spectroscopy opens new research possibilities in the field of laboratory plasma and can lead to a better understanding of thin film synthesis by pulsed laser deposition.

Acknowledgments

The authors wish thank V. García-Gradilla, V. García, and M. Farfán for their technical assistance. Partial support from the Conacyt-México project 400380-5-G36531-E and DGAPA-UNAM projects IN-108696 and IN-102803 is acknowledged.

1. S.S. Harilal, P. Radhakrishnan, V.P.N. Nampoori, and C.P.G. Vallabhan, *Appl. Phys. Lett.* **64** (1994) 3377.
2. D.B. Geohegan, in *Pulsed Laser Deposition of Thin Films*, edited by D.B. Chrisey and G.K. Hubler, Wiley, New York, 1994.
3. D.B. Geohegan, *Thin Solid Films* **220** (1990) 138.
4. H.R. Griem, *Phys. Rev.* **128** (1962) 515.
5. M.A. Gigisos, S. Mar, C. Perez, and I. de la Rosa, *Phys. Rev. E* **49** (1994) 1575.
6. H.R. Griem, *Plasma Spectroscopy*, McGraw-Hill,N.Y. 1997.
7. E. Pérez-Tijerina, J. Bohigas, and R. Machorro, J. *Appl. Phys.* **90** (2001) 3192.
8. S.S. Harilal, C.V. Bindhu, V.P.N. Nampoori, and C.P.G. Vallabhan, *Appl. Phys. Lett.* **72** (1998) 167.
9. J.T. Knudson, W.B. Green, and D.G. Sutton, *J. Appl. Phys.* **61** (1987) 4771.
10. G. Radhakrishnan, P.M. Adams, *Appl. Phys. A* **69** (1999) S33.
11. E. Pérez-Tijerina, J. Bohigas, and R. Machorro, *Rev. Sci. Ins.* **75** 2.
12. A.W. Allen, M. Blaha, W.W. Jones, A. Sanchez, and H.R. Griem, *Phys.Rev. A* **11** (1975) 477.
13. M.S. Dimitrijevic, Z. Djuric and A.A. Mihajlov, *J. Phys. D, Appl. Phys.* 247 (1994) 27.
14. Andor Technology,URL: http://www.andor-tech.com/
15. http://physics.nist.gov/